Atomization and Sprays, vol. 16, pp. 1–16, 2006

EFFECTS OF AIR ON SPLASHING DURING A LARGE DROPLET IMPACT: EXPERIMENTAL AND NUMERICAL INVESTIGATIONS

Richard A. Jepsen
Mechanical Environments, Sandia National Laboratory, P.O. Box 5800, Albuquerque, New Mexico 87185-1135, USA

Sam S. Yoon*
Mechanical Engineering Department, Korea University, Anamdong, 5-Ga, Sungbukgu, Seoul, 136-713, Korea

Byron Demosthenous
Applied Diagnostics, Sandia National Laboratory, P.O. Box 5800, Albuquerque, New Mexico 87185-1135, USA

Original Manuscript Submitted: 07.12.05; Final Draft Received: 11.21.05

Recent studies have shown the importance of air in causing the splashing phenomenon (L. Xu, W. Zhang, and S. R. Nagel, Phys. Rev. Lett., vol. 94, 184505, 2005) and the subsequent finger formation for a large-scale liquid droplet impact. The experimental investigation and the relevant computational modeling have been performed to obtain additional insight on the large-scale splashing phenomenon. Previous modeling efforts did not consider the effect of air by starting the simulation at the time of droplet-liquid contact with the substrate. Here we start the simulation using the volume of fluid method at a location one diameter upstream so that the compressed air effect due to a falling droplet is properly taken into account. Both the experiments and simulations demonstrate that the displaced air obtains momentum from a falling droplet and induces a vortex motion right above the contact surface. The splashing (or ejection) occurs when the initial edge of the impacting and spreading liquid is entrained into the displaced and accelerated air. It is also hypothesized that the perturbation generated during the splashing process is radially propagated and is the fundamental instability that eventually forms fingers at the rim of the spreading liquid.

INTRODUCTION

Droplet impact phenomena are readily encountered in raindrop impact and in numerous industrial applications such as inkjet printing, painting, spray-wall impact within the IC engine, and fire suppression sprays. We are particularly interested in large liquid slug impact and dispersion phenomena, as shown in Fig. 1 [1], where a tank filled with dyed wa-

Sandia is a multiprogram laboratory operated by Sandia Corporation, a Lockheed Martin Company, for the United States Department of Energy's National Nuclear Security Administration under contract DE-AC04-94AL85000. Our sincere thanks go to Prof. Sidney R. Nagel of the University of Chicago for providing the experimental images of Fig. 2. The third author wishes to acknowledge the partial support of this research by a New Faculty Research Grant, funded by Korea University.

*Corresponding author; e-mail: skyoon@korea.ac.kr

ter (2830 kg) impacts an unyielding wall at the speed of 100 m/s; the Weber number for this case is on the order of ~10^8, which far exceeds the previously reported studies limited to We = $\rho D U_{\text{imp}}^2 / \sigma < 5 \times 10^4$ (where ρ, U_{imp}, D, and σ are the liquid density, impact speed, droplet diameter, and liquid surface tension, respectively). These large-scale tests are difficult to repeat and to instrument with the diagnostics necessary to measure details of the fluid structure during breakup and dispersion. Therefore several smaller-scale tests are being performed to investigate the impact and breakup phenomena for large water droplets or slugs (~0.1 m diameter) at large Weber number (1×10^4–1×10^6).

As per well-known classical experiments [2], a droplet is known to stick to the impacting surface at a relatively high impact Weber number when the droplet surface tension energy is not high enough to overcome the droplet's dissipative energy [3]. Upon sticking, the droplet spreads radially and forms a toroidal ring at a relatively low Weber number. At an intermediate Weber number, an azimuthal instability develops and forms "fingers" at the rim of the spreading ring. If the Weber number is increased even more, the droplet "splashes" at the first contact with the surface prior to the finger formation. This transitional behavior, splashing, plays a significant and dominant role in the droplet impact at extremely high impact speed, as in Fig. 1; only splashing occurs without any spreading.

Several fundamental questions remain regarding the droplet impact phenomenon. What causes the splashing and finger formation at the edge of the spreading ring? Is it possible to predict the number of fingers using a linear theory?

The classical Rayleigh-Taylor (R-T) instability [4–6], in which heavy fluid accelerates toward a light fluid, is known to appear as fingers at the fluid-fluid interface. Allen [4] suggested that the observed fingers at the front of the ring of liquid spreading after droplet impact were caused by an R-T instability due to the radial expansion of the liquid into the surrounding air. Although Allen's idea has been accepted among researchers [7–9], Thoroddsen and Sakakibara [10] claimed that the fundamental instability of the fingering phenomenon is due to the initial undulation that imprints on the radially expanding jet at the very first stage of the contact between a falling liquid droplet and the solid substrate.

Recently, Xu et al. [11] reported the importance of air in causing the splashing, which also seemed to affect the fingering instability, as in Fig. 2; when there is no splashing due to the reduced atmospheric pressure, there is no finger formation, and vice versa. Xu et al. [11] stated that splashing occurs because of compressed air while the initially contacted liquid rim flows outward but is pushed back by air resistance, deflecting its mo-

Fig. 1 Dispersed water (dyed red) at furthest extent radially from impact [1]. Frame is ~92 m wide and is 2 s after impact.

tion and resulting in added momentum in the vertical direction. This initial perturbation may be responsible for the finger formation later. The recent experiment by Yoon et al. [12] supported Thoroddsen and Sakakibara's [10] and Xu et al.'s [11] claims on the importance of the initial perturbation due to air by showing that the ejecting splashed liquid is always accelerated by the compressed escaping air, which results in the splashed droplet speed always being greater than the droplet impact speed.

In this article, we present additional experimental data (with respect to Yoon et al. [12]) and examine the compressed air effect on splashing and the subsequent fingering phenomenon using the volume of fluid (VOF) method. The VOF approach was previously used [13–16] for modeling the liquid droplet impact. However, it is important to note that all the previous modeling efforts [13–20] began their simulation at the time on which the impacting droplet was in contact with the substrate, and thus the air effect due to the collapsing droplet cannot be well resolved. Here we start our simulation at a location one diameter upstream from the impacting surface, which has enabled us to computationally investigate the effect of the escaping/accelerated air on splashing.

MODELING

Computational Details

To investigate the dynamics of compressed air, a liquid sphere impacting on a solid surface is simulated using a two-dimensional (2D), two-phase flow, Navier-Stokes (NS) solver (Stormflow, Adaptive Research) that utilizes the conventional VOF method [21]. It

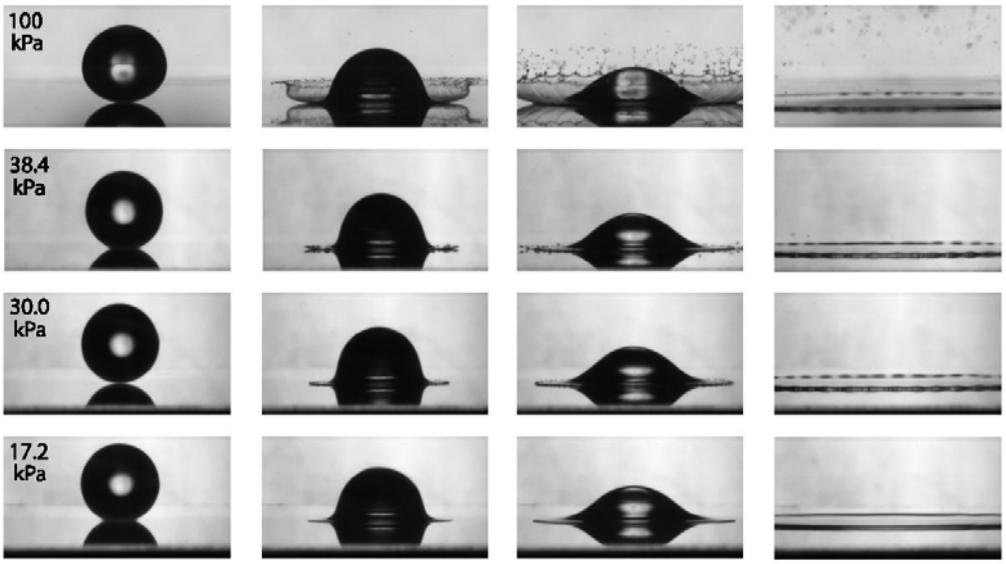

Fig. 2 Recent experiment by Xu et al. [11] of the University of Chicago. Neither the splashing nor finger formation occurred when the atmospheric pressure decreased. Reprinted with the permission of Sidney R. Nagel of the University of Chicago.

is noted that our computation is limited to 2-D and thus is not directly applicable for the actual comparisons with the experimental results. However, it is useful using the current computational tool to obtain qualitative predictions on the behavior of the compressed air due to a falling droplet

The NS solver, based on a Reynolds-averaged Navier Stokes (RANS) formulation employing a standard $k - \varepsilon$ isotropic turbulence closure model of Nallasamy [22], is coupled with the Lagrangian droplet tracking model [23, 24]. The gas-phase flow is calculated on a Eulerian staggered Cartesian mesh using the pressure correction method of the SIMPLEC algorithm [25]. The second-order upwinding and centered scheme are used for the convective and diffusion terms, respectively, in solving the transport differential equations. The droplet phase evolves using a Lagrangian approach based on the stochastic separated flow model [23, 24]. The momentum equation for a small, rigid sphere in a nonuniform flow of Maxey and Riley [26] is used, and the drag model of Faeth [23] is used.

The computational domain for our simulation extends 0.6 m × 0.3 m using a 190 × 94 mesh resolution that is symmetric about the droplet center line. The computational node is carefully chosen after the verification of the solution independence from the mesh resolution. The diameter of the impacting droplet is 0.1 m, and the impact speed is 10 m/s. The mesh resolution in the droplet impact area (0.1 m × 0.1 m) was refined to 50 × 50 cells. The time step for the calculation was 2×10^{-5} s. Most of the parametric runs require the computational time of less than 1 day on a PC with 2.4-GHz processor. The stair-step mesh is applied to resolve the smooth circular shape of the droplet in a Cartesian coordinate system. This stair-step mesh is unavoidable in the VOF method, as mentioned by Pasandideh-Fard et al. [16] and Bussmann et al. [7], unless the method is timely modified by or coupled with the finite element method [18] or boundary integral method [19, 20]. The computational mesh is extended up to six and three diameters in horizontal and vertical directions, respectively, as shown in Fig. 3. Since the computational results are based

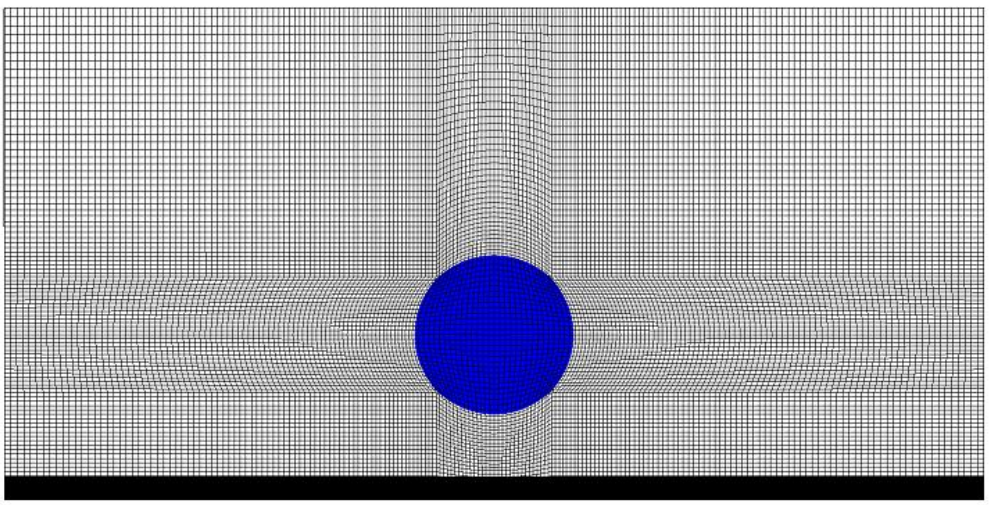

Fig. 3 Falling droplet prior to impact in a computational mesh.

on the 2D mode, the direct comparison against the experiment cannot be made. It is noted that the objective of Section 2 is to provide an insight on the mechanism of the compressed/accelerated air caused by a falling droplet for the benefit of the discussion on the experiment in Section 3. It is reiterated that the previous modeling efforts [13–20] did not account for the accelerated air effect because the simulated droplet was in contact with the solid surface at the beginning of their simulations. We start our simulation at a location one diameter upstream from the impacting surface, which has enabled us to computationally investigate the effect of the escaping/accelerated air on splashing.

Entrainment of Water from Accelerated Air

In Fig. 4, the time series of an impacting droplet is shown. Prior to the impact, the air is compressed and accelerated up to 5 times the impact speed (U_{imp} = 10 ± 0.5 m/s) at t = 0. It is clear that the air obtained an upward vertical momentum while being compressed due to a downward-falling droplet. At t = 2 ms, an induced vortex roll-up motion of air is

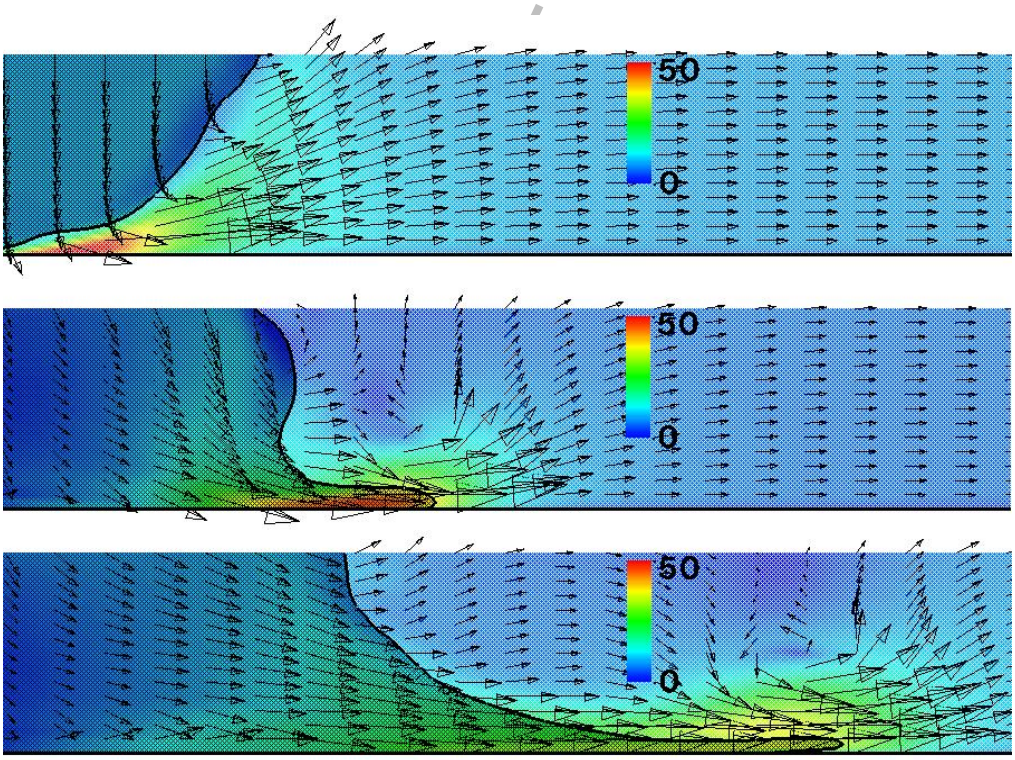

Fig. .4 Evolution of the induced air due to a falling droplet at t = 0, 2, and 4 ms. The unit for the contour level is meters per second. The maximum speed of the induced air nears 5 times the impact speed (i.e., U_{imp} = 10 m/s, D = 0.1 m). The color contour is scaled with the local total velocity. The light and dark regions represent the air and liquid, respectively. Note that the domain shown extends 15 cm × 3 cm. The VOF, $(\rho_{cell} - \rho_{gas})/\rho_{liq}$, value used in this contour plot is 0.5

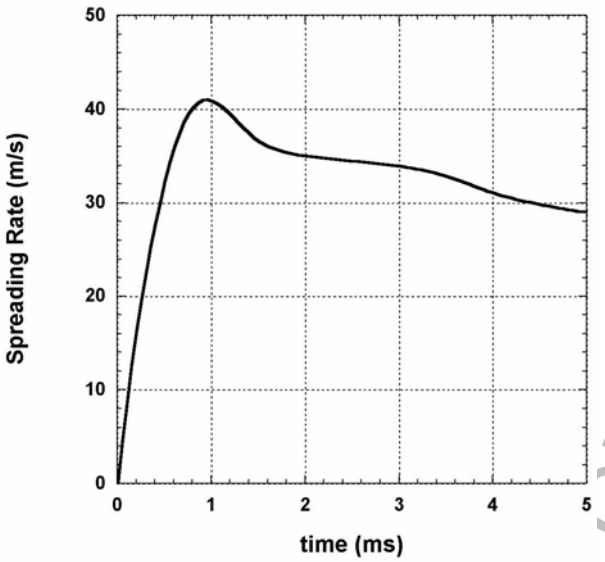

Fig. 5 Spreading rate of impacting droplet shown in Fig. 4 using a VOF of 0.5 for the interface at the leading edge.

observed due to spreading liquid. This roll-up motion continues to follow the edge of the spreading liquid at t = 4 ms. At this point, the air reduces its speed because the air is no longer displaced under the fluid. However, the fluid still affects the air motion (especially the air layer in contact with the moving fluid) while spreading radially. In Fig. 5, the liquid spreading speed of the case shown in Fig. 4 is recorded. It is shown that the liquid quickly obtains momentum within 1 ms, and thus the fluid edge is accelerated. For 1 ms < t < 5 ms, the fluid edge decelerates because the boundary layer effect starts to dominate and impede the motion of the liquid spreading. This impeding motion of the boundary layer effect is later (t > 5 ms) compared to the fast-traveling, multiple-bouncing waves, of which discussion will be introduced in Section 3.

To estimate the ejection intensity of the compressed air, we have located a few liquid particles of a constant size directly under the droplet center with an initial velocity of zero. It is expected that the smaller droplets' motion will be readily entrained by the es-

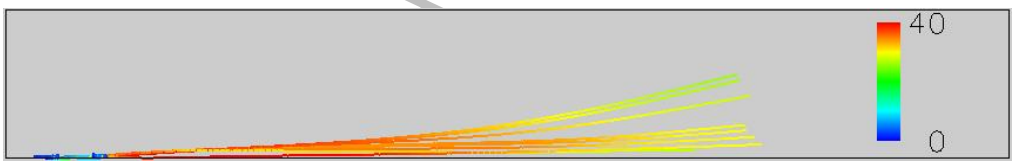

(a) Dpart = 0.50 mm

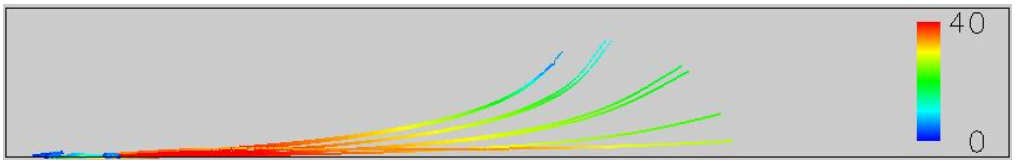

(b) Dpart = 0.25 mm

Fig. 6 Path lines of the ejected particles from initial ejection up to t = 8 ms for various particle sizes, (a) D_{part} = 0.50 mm and (b) D_{part} = 0.25 mm, in conjunction with Fig. 4 and Table 1. Ten particles were ejected. The color contour is scaled with the Lagrangian total droplet velocity. Note that the particle size of D_{part} = 1.0 mm (which is not shown in this figure) did not gain any vertical momentum due to its heavy weight. The domain shown extends 40 cm × 6 cm. The lower left corner is the center of the impacting droplet, as in Fig. 4. Note that the atmospheric pressure is 100 kPa. The impact speed is 10 m/s.

Table 1 Statistics of the Traveling Particle of Various Sizes

Particle size, mm	Δy_{max}, mm	U_{max}, m/s
0.25	47	45
0.50	34	42
1.00	5	26
2.00	<1	19

The droplet size and impact speed are 0.1 m and 10 m/s, respectively.

Table 2 Statistics of the Traveling Particle at Various Atmospheric Pressures

Atmospheric pressure, kPa	Δy_{max}, mm	U_{max}, m/s
100	47	45
70	21	39
50	9	22
30	2	19

The ejecting particle size is 0.25 mm. The droplet size and impact speed are 0.1 m and 10 m/s, respectively.

caping, accelerated air, whereas the motion of the larger droplets will not be as intense as that of the smaller droplets. The motions of D_{part} = 0.50-mm and 0.25-mm particles shown in Fig. 6 indicate that the results are consistent with the expected behavior; the smaller particles (D_{part} = 0.25 mm, as in Fig. 6b) are lifted higher than the larger particles. Table 1 shows the maximum lifted height (Δy_{max}) and the maximum speed (U_{max}) of the particles ranging 0.25 mm < D_{part} < 2.00 mm. The particles, initially at rest, are accelerated (see the change in contour level from blue to red in Fig. 6) with the compressed air, and then their speed is reduced due to air drag. This difference in the dynamic behavior due to the change in the particle size confirms that the accelerated air is capable of entraining and lifting small droplets, but the large particles will not be as significantly affected. These parametric studies also confirm that the compressed air is the fundamental cause for the fast-traveling splashed droplet upon impact. In addition, the vortex roll-up at the leading edge of the interface may also contribute to the splash crown formation.

The ability of the escaping air to entrain and lift a liquid particle is also affected by pressure. A lower air pressure results in a lower air density that is not as capable of transferring momentum to the spreading liquid or splashing particles. It should be noted that the escaping air has the same velocity in all cases since it is driven by the relative change in pressure between the compressed region near the impact and the surrounding ambient pressure. Table 2 summarizes the model results for the same particle size at progressively lower pressures (and densities). Model results show that the particles experience greatly reduced lift and entrainment as the pressure decreases. This trend is also consistent with the experimental findings of Xu et al. [11].

EXPERIMENT

Experimental Apparatus

Large water slug impact experiments were done using latex bladders (balloons) to transport the slugs to a clear acrylic target. Immediately prior to impact, the latex was re-

(a) **(b)**

Fig. 7 (a) Capturing the side view. (b) Gas cloud generation using dry ice. A balloon droplet is released onto the stabilized region (upper right corner).

moved using a small (0.5 cm) blade. The latex peels away from the water in less than 1 ms, resulting in a large, spherical water droplet shaped like the latex bladder. No effects of the bladder remain when the droplet impacts the target (the reasons are well explained in Yoon et al. [12]).

Data was gathered using three digital Phantom cameras (Vision Research, Wayne, NJ), arranged as shown in Fig. 7a, with frame rates between 4800 and 10,000 fps and exposure times from 5 to 100 μs per frame. Both forward and backlighting techniques were used. A thin CO_2 cloud layer in Fig. 7b and glitter particles were used to observe their induced motion upon the droplet impact. TrackEye software was used to postprocess the time history of the velocity of the ejecting fluid particles upon splashing. Droplet size was fixed at $D = 0.1$ m, and the drop height varied from 1.27 m to 1.94 m, which gives the impact speed of $U_{imp} = 5 \pm 0.25$ m/s and 6.18 ± 0.31 m/s.

Experimental Results

In Fig. 8, the splashed droplets and the spreading fluid ring are shown. Using the TrackEye software, the radial velocities of randomly chosen droplets (splash 1, splash 2, and splash 3) are recorded, as in Fig. 9a. The start time for the tracking in Fig. 9a was 7–27 ms after impact because the particles or spreading edge were not easily discernable at early times due to the interference and high density of splashing particles. However, all three splashed droplets show some minor acceleration ("Λ" shape) at the initial stage and then experience an air drag, and thus their velocities reduce. The pattern of the spreading edge or ring velocity appears to be quite interesting as its value fluctuates during its spreading for the period of 28 ms $< t <$ 45 ms. The fluctuation may be due to the pressure pulsing generated during the continuous supply of the impacting fluid. In Fig. 9b, the liquid spreading velocity from the modeling prediction (which is in conjunction with the experiment shown in Fig. 9a) is shown. This modeling prediction also indicates the rapid acceleration within 2 ms and the appearance of the fluctuation starting from approximately $t = 23$ ms up to $t = 34$ ms; any further recording was not possible due to the computational domain limit used for this modeling run.

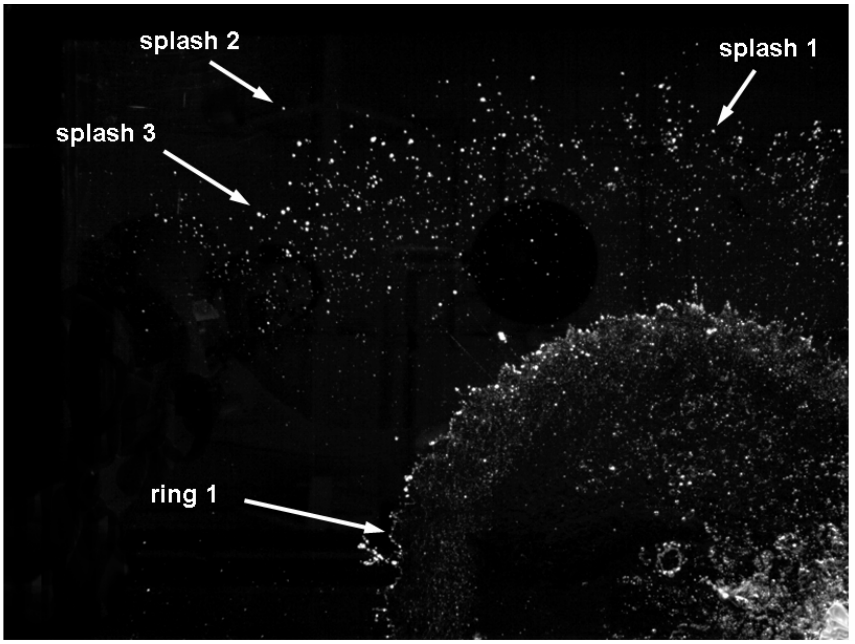

Fig. 8 Splashing droplets and the spreading fluid ring upon impact. Photo taken beneath the transparent plexiglass focusing on the quadrant view. The operating conditions are $U_{imp} = 5 \pm 0.25$ m/s, $D = 0.10$ m.

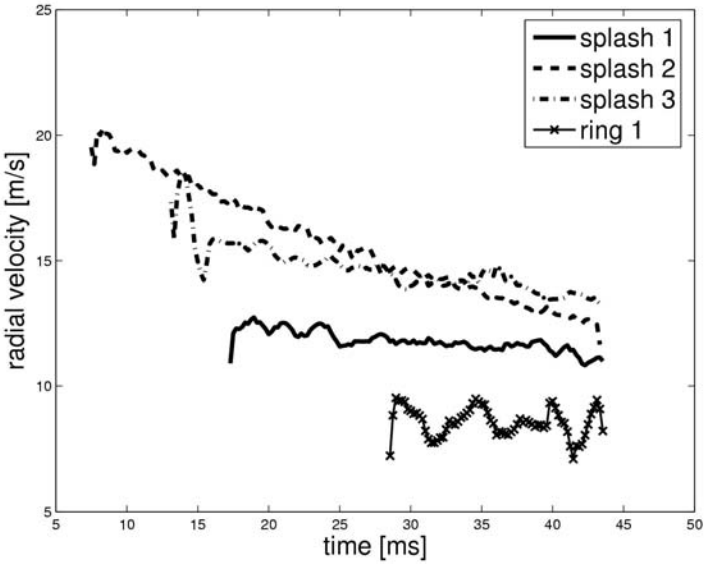

(a)

Fig. 9 Spreading ring velocity ("ring 1" in the legend box): (a) from the experiment shown in Fig. 8.

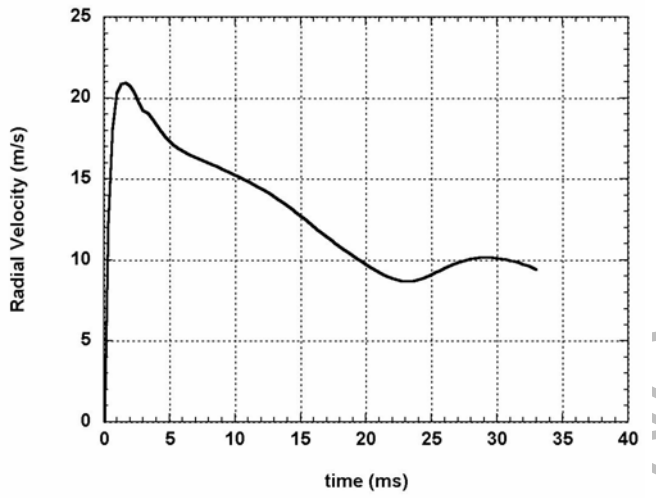

(b)

Fig. 9 (cont'd) (b) modeling prediction on the "ring" radial velocity (using the VOF model).

It is interesting to observe that the maximum radial velocity is ~4 times the impact velocity (i.e., U_{imp} = 5 ± 0.25 m/s and $U_{rad,\ max}$ ~ 20 ± 1 m/s). This trend is consistent with the case shown in Figs. 4 and 5: U_{imp} = 10 ± 0.5 m/s and $U_{rad,\ max}$ ~ 40 ± 2 m/s. It is noteworthy that the maximum spreading radial velocity is always smaller than the maximum velocity of the accelerated/escaping air: $U_{air,\ max}$ ~ 50 ± 2.5 m/s from Fig. 4.

Figures 10–12 show the evolution of the induced motion of the compressed air during the collapsing phase of a falling droplet on a thin layer of CO_2 on the target surface. The photos were taken from beneath the transparent plexiglass (Figs. 10 and 11) and from the side (Fig. 12) for the same event. In this case, the latex on the balloon was not removed so that the water splashing would not interfere with the air-gas interactions. Certainly, the balloon rebounds subsequent to the impact due to the excessively high surface tension force of the latex. Three very important observations should be noted from these tests. One is that the CO_2 gas is displaced ahead of the leading edge of the deformed impacting droplet (Figs. 10 and 11); second is that a crown shape (3-D instability) appears due to the vortex roll-up of the escaping air as the similar crown shape was formed (Fig. 12) by the splashing liquid droplet in Fig. 2 (see 100-kPa case); and finally, there appears to be a sunflower-shaped 3-D instability induced from the escaping air (Fig. 11).

Tests were also done to investigate the ability of the escaping air to entrain particles initially at rest in the impact region. Figure 13 shows the effect on aluminum glitter particles due to the escaping air from the impact. Here the latex was also allowed to stay intact so that the splashing water would not interfere with the observation. The results show the glitter particle being ejected and lifted from the target surface in a crown-shaped pattern when accelerated by the escaping air.

The velocity and lift of the glitter particles is less than predicted from the water particle simulation because the glitter particles are aluminum and are almost 3 times denser. However, the qualitative pattern is very similar to that of water splashing.

It is worthy to reiterate the objective of our current study. It is claimed, in this report, that the surrounding air has a profound effect on splashing. As mentioned previously, the splashing acts as an initial perturbation for the eventual finger formation during the liquid spreading on the impact surface, whereas the conventional thought contrarily suggests that

the spreading itself causes the finger formation due to the R-T instability. To prove our claim, we focus our attention on the initial perturbation, which we believe to be the fundamental cause of splashing. It is natural to believe that there must be some interaction between the falling droplet and the accelerated air.

Certainly the air below the falling droplet is compressed, and thus the air density changes slightly (but the change does not exceed orders of magnitude). The shearing effect between the falling droplet and the rapidly escaping air might be significant enough to cause some disturbance at the bottom of the falling droplet and becomes the source of the initial undulation that Thoroddsen and Sakakibara [10] observed in their experiment. To show our point, we examine the wave numbers of the maximum growth rate from both the R-T instability and the Kelvin-Helmholtz instability [27].

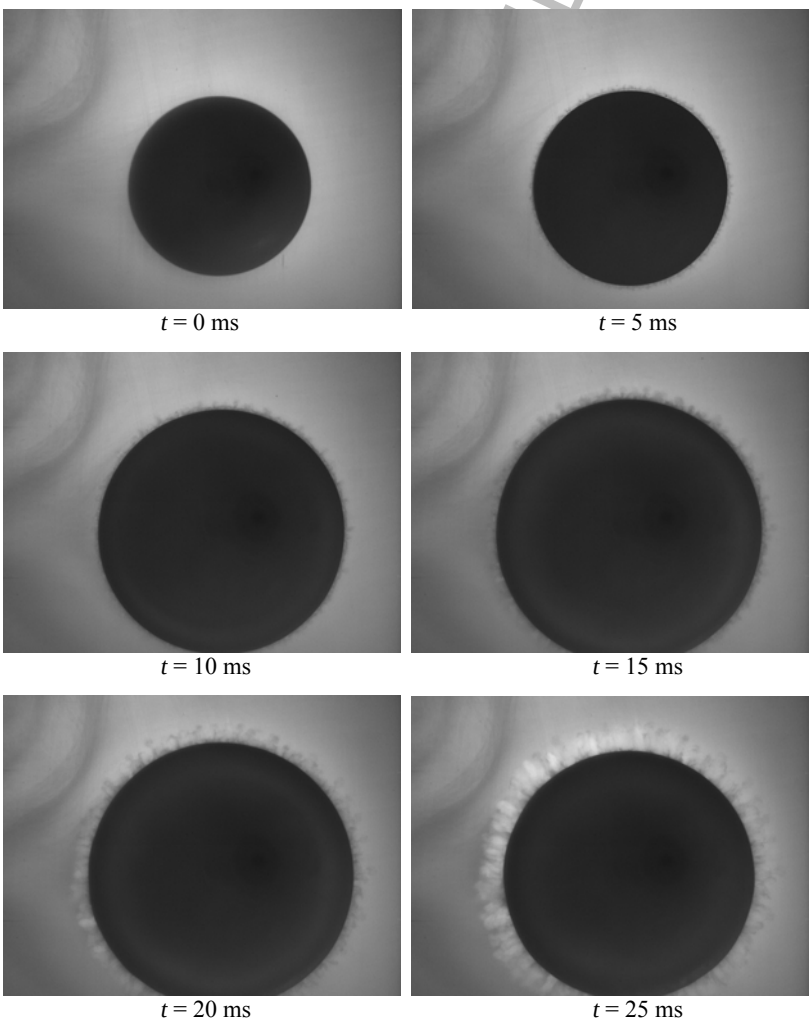

Fig. 10 Evolution of the finger formation due to the induced azimuthal instability of air when a balloon hits the plexiglass surface. Photos are taken beneath the plexiglass at the bottom location.

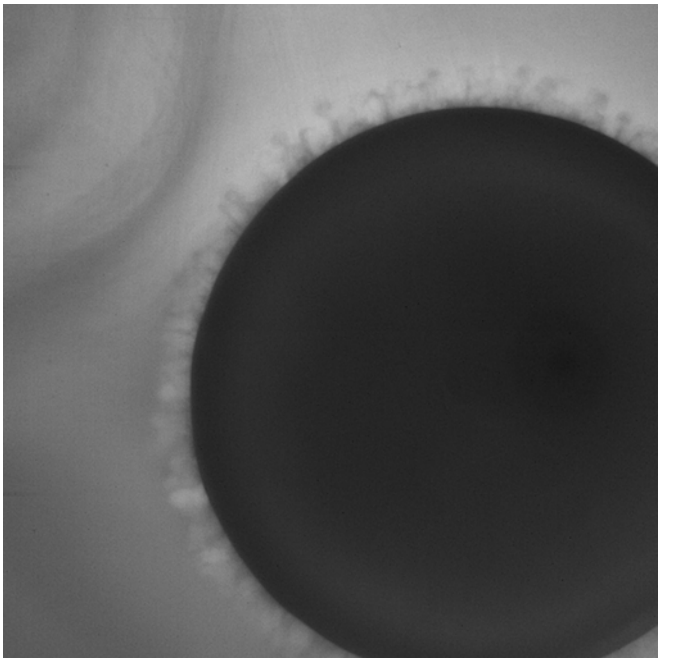

Fig. 11 Magnified view of Fig. 10 at t = 15 ms on which the spreading diameter is at maximum.

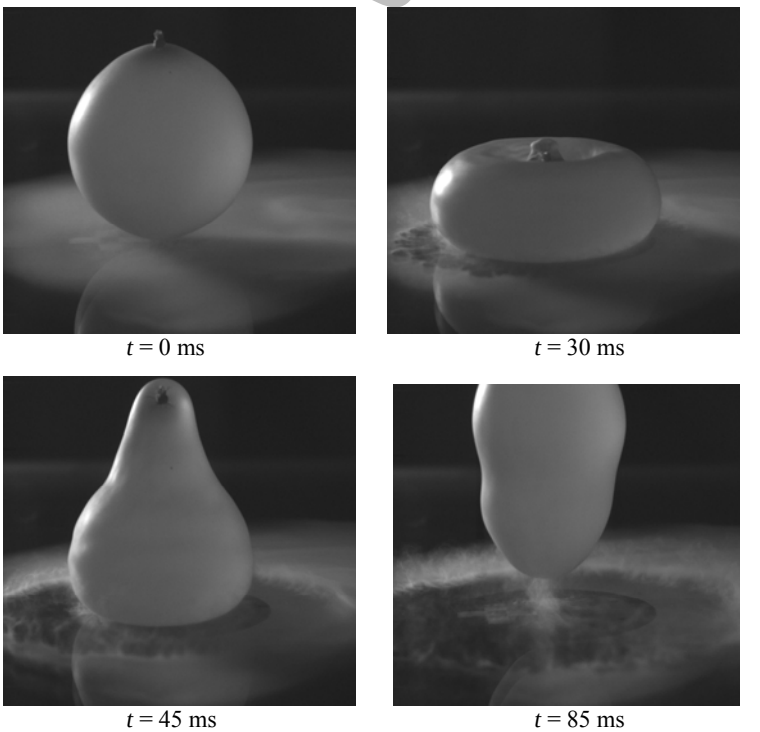

Fig. 12 Side view of the experiment corresponding to Fig. 10. The balloon droplet rebounds due to its high surface tension energy.

The dispersion relation from the R-T instability is as below [4, 6]:

$$\omega^2 = \frac{\rho_l - \rho_g}{\rho_l + \rho_g} gk - \frac{\sigma}{\rho_l + \rho_g} k^3 \tag{1}$$

where g is the acceleration/deceleration of the liquid spreading edge upon impact. The subscripts g and l represent the properties of gas and liquid, respectively. The maximum wave number, k_{max}, corresponding to the maximum growth rate, ω_{max}, can be found by taking the derivative of Eq. (1) with respect to the wave number, k, and setting the derivative equal to zero:

$$k_{max} = \sqrt{\frac{g(\rho_l - \rho_g)}{3\sigma}} \tag{2}$$

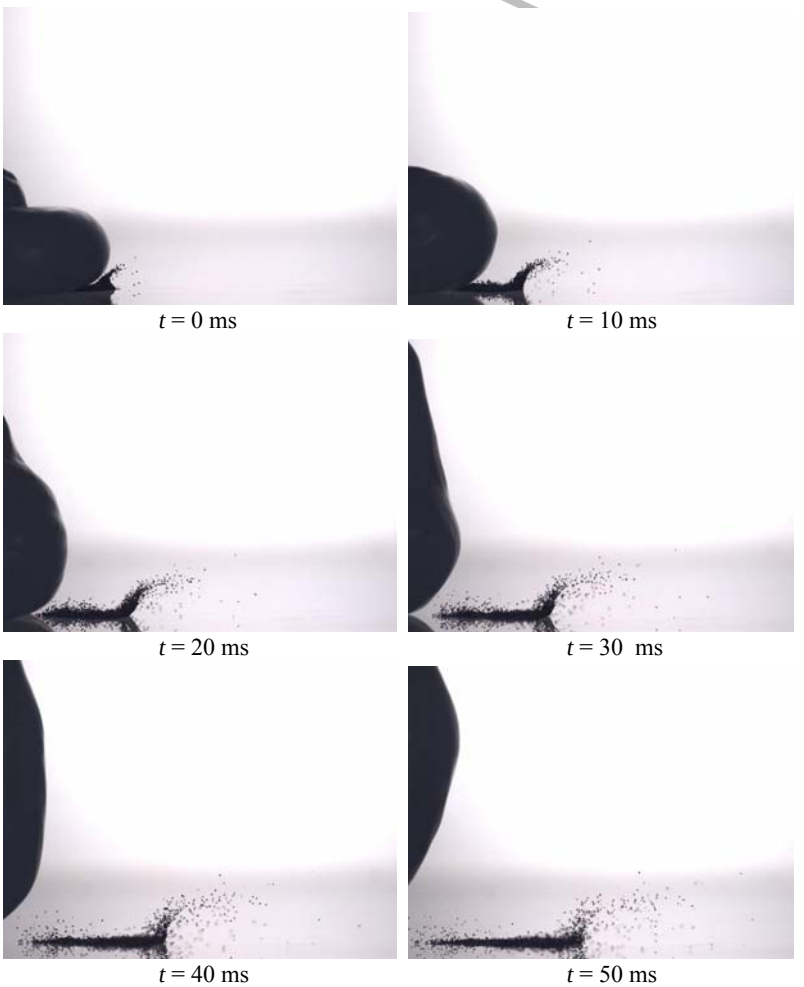

Fig. 13 Ejection of the glitter particles due to the compressed accelerated air upon impact.

Although the dispersion relation of the Kelvin-Helmholtz instability in the limiting case of $ka \to \infty$ and $\rho_g \ll \rho_l$ is written as follows:

$$\omega^2 = \frac{\rho_g}{\rho_l} U_{\text{rel}}^2 k^2 - \frac{\sigma}{\rho_l} k^3 \tag{3}$$

(where U_{rel} is the relative velocity between the liquid and air), the maximum wave number of the Kelvin-Helmholtz instability can be obtained in the same manner as applied to the R-T instability above:

$$k_{\max} = \frac{2}{3} \frac{U^2 \rho_g}{\sigma} \tag{4}$$

These maximum wave numbers in Eqs. (2) and (4) are plotted as a function of the gas density, ρ_g, as in Fig. 14. The gas density varies from 1 kg/m^3 (air density) to 1000 kg/m^3 (water density). The Xu et al. [11] droplet characteristics are chosen for this comparison: The droplet diameter is 3.4 mm, and the impact speed is 3.74 m/s. The deceleration of the spreading liquid is approximated by $g \approx U_{\text{imp}}^2 / D$, according to Aziz and Chandra [3]. The initial relative velocity between the falling droplet and the escaping air should be 5 times the impact speed, according to the modeling observation from Fig. 4. However, the ratio between the relative and impact velocities is varied from 1 to 4 for a conservative estimate.

When taking the limit of $\rho_g \to 0$ for the case of a vacuum to be consistent with the experiment of Xu et al. [11], the R-T wave number indicates that the mode is still unstable as the maximum wave number is positive, which is contrary to the experimental observation [11]. On the other hand, the wave number of the Kelvin-Helmholtz instability indicates that the mode is absolutely stable as $k_{\max} \to 0$ in the limit of $\rho_g \to 0$, which is consistent with Xu et al.'s [11] observation. In addition, the R-T theory cannot explain the sudden change of the stability mode observed in the experiment of Xu et al. [11] when the gas density changed from 1 kg/m^3 to $\rho_g \to 0$ (i.e., vacuum), whereas the Kelvin-Helmholtz theory does explain the quickly changing char-

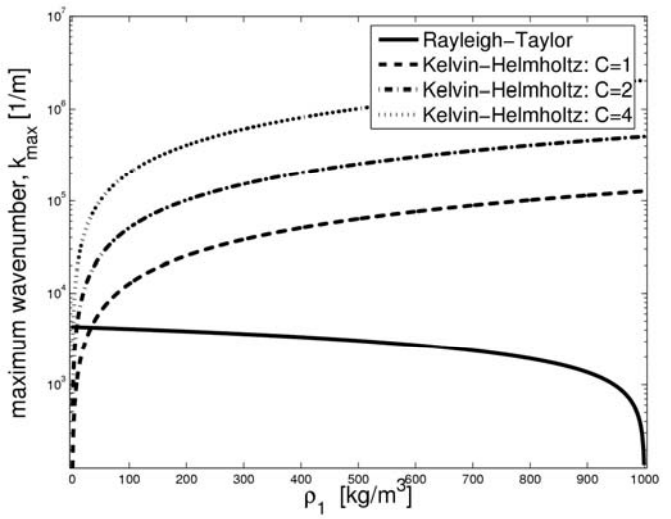

Fig. 14 Maximum wave number comparison between the Rayleigh-Taylor and Kelvin-Helmholtz theories at various gas densities, ρ_g. Xu et al.'s [11] droplet is considered for this comparison: The droplet diameter is 3.4 mm, and the impact speed is 3.74 m/s. For the Rayleigh-Taylor instability, the deceleration is approximated as $g \approx U_{\text{imp}}^2 / D$ according to Aziz and Chandra [3]. For the Kelvin-Helmholtz instability, the ratio between the air escaping speed and the impact speed is taken to be $C = U_{\text{rel}}/U_{\text{imp}} = 1$, 2, and 4.

acteristics of the instability mode for the sudden gas density change as ρ_g nears zero. Most liquid impact tests have been tested in the atmospheric condition where the gas density is 1 kg/m^3, whose wave number spectrum is shared by both the R-T instability and the Kelvin-Helmholtz instability, as shown in Fig. 14. It may be coincidence that the experimental data were in agreement with the Rayleigh-Taylor instability because it shares the same spectrum region on Fig. 14 as the Kelvin-Helmholtz instability curves. At this point, we cannot absolutely conclude that the Kelvin-Helmholtz instability is the fundamental cause of splashing due to lack of experimental data. It would certainly be interesting to compare the experimental data obtained in the higher gas density environment (such as argon or nitrogen) with the instability theories mentioned above and identify the true instability theory that explains the fundamental cause of splashing.

CONCLUSION

Both model simulation and experimental results demonstrate that the compressed and displaced air directly beneath the impacting droplet affect the splashing and spreading characteristics. Model simulations show the escaping air traveling as much as 5 times the droplet impact velocity and creating a vortex roll-up that moves radially away from the impact region near the spreading liquid-air interface. Simulations also show that the fast-moving air is capable of enough momentum transfer to entrain small droplets into the ejected air and even follow the vortex roll-up. However, our model shows that air at reduced pressure and density has much less ability to entrain the liquid. Likewise, the same phenomena are quantitatively supported by experimental data. The experiments also suggest that the instability that forms fingers in the spreading liquid may be something other than the R-T instability traditionally believed. We suggest that the Kelvin-Helmholtz may be the fundamental source of the instability, which certainly deserves the attention of the liquid impact research community for further investigation. Many of the claims in this article have not been observed in previous work because the simulations in the past started with the droplet already in contact with the surface and did not allow for any compressed or displaced air. In addition, our simulations and experiments are at a much higher Weber number, whereby the splashing and spreading phenomena discussed here are more pronounced.

REFERENCES

1. R. A. Jepsen, K. Jensen, and T. O'Hern, Water Dispersion Modeling and Diagnostics for Water Slug Impact Test, *SEM X Int. Congress*, 2004.
2. A. M. Worthington, On the Forms Assumed by Drops of Liquids Falling Vertically on a Horizontal Plate, *Proc. R. Soc. London*, vol. 25, pp. 26, 1877.
3. S. D. Aziz and S. Chandra, Impact, Recoil and Splashing of Molten Metal Droplets, *Int. J. Heat Mass Transfer*, vol. 43, pp. 2841–2857, 2000.
4. R. F. Allen, The Role of Surface Tension in Splashing, *J. Colloid Interface Sci.*, vol. 51, pp. 350–351, 1975.
5. D. H. Sharp, An Overview of Rayleigh-Taylor Instability, *Physica D*, vol. 12, pp. 3–18, 1984.

6. S. Chandrasekha, *Hydrodynamic and Hydromagnetic Stability*, Oxford University Press, London, 1961.
7. M. Bussmann, S. Chandra, and J. Mostaghimi, Modeling the Splash of a Droplet Impacting a Solid Surface, *Phys. Fluids*, vol. 12, pp. 3121–3132, 2000.
8. H. Y. Kim, Z. C. Feng, and J. H. Chun, Instability of a Liquid Jet Emerging from a Droplet upon Collision with a Solid Surface, *Phys. Fluids*, vol. 12, pp. 531–541, 2000.
9. N. Z. Mehdizadeh, S. Chandra, and J. Mostaghimi, Formation of Fingers around the Edges of a Drop Hitting a Metal Plate with High Velocity, *J. Fluid Mech*., vol. 510, pp. 353–373, 2004.
10. S. T. Thoroddsen and J. Sakakibara, Evolution of the Fingering Pattern of an Impacting Drop, *Phys. Fluids*, vol. 10, pp. 1359–1374, 1998.
11. L. Xu, W. Zhang, and S. R. Nagel, Drop Splashing on a Dry Smooth Surface, *Phys. Rev. Lett.*, vol. 94, 184505, 2005.
12. S. S. Yoon, R. A. Jepsen, M. R. Nissen, and T. J. O'Hern, Experimental Investigation on Splashing and Nonlinear Fingerlike Instability of Large Water Drops, *J. Fluids Struct.* (in press), 2006.
13. G. Trapaga and J. Szekely, Mathematical Modeling of the Isothermal Impingement of Liquid Droplets in Spraying Processes, *Metall Trans. B*, vol. 22, pp. 901–914, 1991.
14. G. Trapaga, E. F. Matthys, J. J. Valencia, and J. Szekely, Fluid Flow, Heat Transfer, and Solidification of Molten Metal Droplets Impinging on Substrates: Comparison of Numerical and Experimental Results, *Metall. Trans. B*, vol. 23, pp. 701–718, 1992.
15. H. M. Liu, E. J. Lavernia, and R. H. Rangel, Numerical Simulation of Substrate Impact and Freezing of Droplets in Plasma Spray Processes, *J. Phys. D*, vol. 26, pp. 1900–1908, 1993.
16. M. Pasandideh-Fard, Y. M. Qiao, S. Chandra, and J. Mostaghimi, Capillary Effects During Droplet Impact on a Solid Surface, *Phys. Fluids*, vol. 8, pp. 650–659, 1996.
17. G. B. Foote, The Water Rebound Problem: Dynamics of Collision, *J. Atmos. Sci.*, vol. 32, pp. 390–402, 1975.
18. J. Fukai, Z. Zhao, D. Poulikakos, C. M. Megaridis, and O. Miyatake, Modeling of the Deformation of a Liquid Droplet Impinging upon a Flat Surface, *Phys. Fluids A*, vol. 5, pp. 2588–2599, 1993.
19. A. L. Yarin and D. A. Weiss, Impact of Drops on Solid Surfaces: Self-Similar Capillary Waves, and Splashing As a New Type of Kinematic Discontinuity, *J. Fluid Mech.*, vol. 283, pp. 141–173, 1995.
20. M. R. Davidson, Boundary Integral Prediction of the Spreading of an Inviscid Drop Impacting on a Solid Surface, *Chem. Eng. Sci*., vol. 55, pp. 1159–1170, 2000.
21. C. W. Hirt and B. D. Nichols, Volume of Fluid (VOF) Method for the Dynamics of Free Boundaries, *J. Comput. Phys.*, vol. 39, pp. 201–225, 1981.
22. M. Nallasamy, Turbulence Models and Their Applications to the Prediction of Internal Flows: A Review, *Comput. Fluids*, vol. 15, pp. 151–194, 1987.
23. G. M. Faeth, Evaporation and Combustion in Sprays, *Prog. Energy Combust. Sci.*, vol. 9, pp. 1–76, 1983.
24. G. M. Faeth, Mixing, Transport and Combustion in Sprays, *Prog. Energy Combust. Sci.*, vol. 13, pp. 293–345, 1987.
25. S. V. Patankar, *Numerical Heat Transfer and Fluid Flow*, Taylor and Francis, New York, 1980.
26. M. R. Maxey and J. J. Riley, Equation of Motion for a Small Rigid Sphere in a Non-uniform Flow, *Phys. Fluids*, vol. 26, pp. 883–889, 1983.
27. S. S. Yoon and S. D. Heister, Categorizing Linear Theories for Atomizing Round Jets, *Atomization and Sprays*, vol. 13, pp. 499–516, 2003.